

Numerical Study of Variable-Camber Wing via Drag Decomposition Method

Wei Niu, Haixin Chen*, Yufei Zhang* and Miao Zhang***

**School of Aerospace Engineering, Tsinghua University, Beijing, 100084, China
chenhaixin@tsinghua.edu.cn*

*** Shanghai Aircraft Design and Research Institute, Shanghai, 201210, China
zhangmiao@comac.cc*

Abstract

The variable-camber wing technology is a useful way to improve the aerodynamic performance of airplane. In order to fully understand and utilize this technology, more researches need to be done. This paper studies the impact of trailing-edge variable-camber wing on the aerodynamic drag and the drag components by numerical simulation. A far-field drag decomposition method based on CFD is used for study. The numerical calculations have revealed the inner relation between trailing edge camber of wing and aerodynamic drag. The research results are helpful to the design of variable-camber wing.

1. Introduction

In recent years, the civil aviation market is growing rapidly. Almost all the civil jet airplanes are designed based on the traditional three-segment wing layout, which includes the leading-edge slat, the main wing and the trailing-edge flap [1]. The traditional wings have been designed and used for nearly sixty years. New design techniques improved the performance of traditional wing dramatically [2], and also made the traditional wing more and more mature, which means it is hard to further improve the performance of the traditional wings.

In order to survive under drastic competition, airplanes manufacturers must find new ways to improve the performance of the traditional wings [3]. The variable-camber wing technology is one of the ways that can achieve the goal. This technology allows the wings to change its camber during flight [4], which helps the traditional wings overcome the weaknesses. In the design process of airplanes, designers usually takes multiple flight conditions into consideration. Different flight conditions have different requests of aerodynamic geometry [5]. However, the traditional wings keep fixed shape in climb, descend and cruise phases, which means the traditional wings are unable to satisfy all the flight conditions. The variable-camber wings will have different aerodynamic shapes in different flight conditions, which helps the wings overcome the conflicts and have better performance in different flight phases [6]. Many research have been done to study the effect of variable-camber wing [7-14].

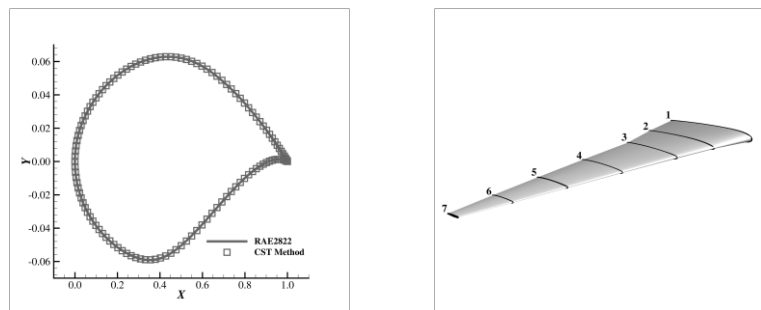
In this paper, we study the aerodynamic characteristics of trailing-edge variable-camber wing. The variable-camber wing technology improves the aerodynamic performance of airplanes by two ways. First, it adjusts the chordwise pressure distribution of wing surface and weaken the shock wave. Second, it adjusts the spanwise load distribution to reduce the induced drag. Revealing the specific working mechanism of variable-camber wing technology will be helpful for design and research. However, due to the complexity of air flow, the changes of pressure distribution and load distribution are coupled together, making it hard to distinguish the variation of wave drag and induced drag. Consequently, a drag decomposition method based on CFD is used for analyzing the changes of drag

components [15]. A two-dimensional supercritical airfoil and a three-dimensional supercritical wing are selected for research. Through the numerical simulations, the impacts of trailing-edge variable-camber wing on different drag components are studied.

2. Numerical Method

2.1 Parameterization Method

The class-shape transformation (CST) method (Eq.(1)) is used for the parameterization of the airfoil and the wing [16]. This method is composed of a class function and a shape function, as shown in Eq.(2) and Eq.(3). The class function roughly describes the geometry. The shape function adjusts the detailed shape. The results of CST method is shown in Figure 1 (a). The supercritical wings are controlled by seven airfoil sections. The 3-order spline interpolation method is used for generation of wing geometry, as shown in Figure 1 (b).



(a) Airfoil created by CST (b) Wing Created by CST and interpolation

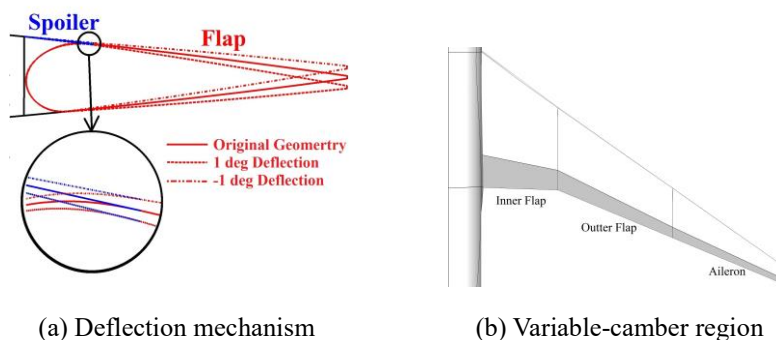
Figure 1: Class-Shape Transformation Method

$$Y(x/C) = C_{N1}^{N2}(x/C) \times S(x/C) \quad (1)$$

$$C_{N1}^{N2}(x/C) = (x/C)^{N1}(1 - x/C)^{N2} \quad (2)$$

$$S(x/C) = \sum_{i=0}^6 b_i B_i^k(x/C) \quad (3)$$

In this paper, we use the flaps and spoilers to achieve the trailing-edge variable-camber function. The wing adjusts its trailing-edge camber by rotating the flaps, while the spoilers are attached to the upper surface of flap to maintain the continuity of wing, as shown in Figure 2 (a) (clockwise rotation is positive). For most civil airplane, there are two individual flap, as shown in Figure 2 (b). We assume the flaps is able to alter the camber independently.



(a) Deflection mechanism (b) Variable-camber region

Figure 2: The mechanism of variable-camber wing

2.2 Drag decomposition Method

A far-field drag decomposition method based on CFD is selected for analyzing the drag components of trailing-edge variable-camber wings. This method calculate the value of drag components by volume integral. For a two-dimensional airfoil without momentum source, the drag acting on arbitrary closed surface is written as Eq.(4). The p , ρ , τ_x , u , \vec{V} refer to the pressure, density, viscous force, velocity and velocity component in X-direction, respectively.

$$D_{far} = \iint_{s_{far}} (-pn_x + \tau_x \cdot \vec{n} - \rho u(\vec{V} \cdot \vec{n})) dS \quad (4)$$

The approximate hypotheses and Gauss' law convert Eq.(4) into Eq.(5), where the drag becomes the volume integral of drag source $\vec{\nabla} \cdot \vec{F}_{irrev}$. The $\vec{F}_{irrev} = -\Delta u_{irrev} \rho \vec{V}$, and Δu_{irrev} refers to the velocity change caused by irreversible process.

$$D_{far} = \iiint_{V_{far}-V_{near}} \vec{\nabla} \cdot \vec{F}_{irrev} dV \quad (5)$$

By dividing the drag integral region, the drag decomposition method is able to calculate drag components through volume integral. In this paper, Eq.(6) [17] and Eq.(7) [18] are used to separate viscous region and shock wave region, respectively. The viscous region and shock wave region are shown in Figure 3 (a) and Figure 3 (b).

$$f_{wave} = \frac{\vec{\nabla} \cdot \vec{\nabla} P}{a \cdot |\vec{\nabla} P|} \quad (6)$$

$$f_{viscous} = \log_{10}(\rho \varepsilon / Ma_{\infty}^3) \quad (7)$$

Induced drag comes from the wingtip vortex. The downstream flow field of wingtip is classified as induced drag region. The integral of $\vec{\nabla} \cdot \vec{F}_{irrev}$ in this region and the kinetic energy of wingtip vortex at downstream will be used to calculate the induced drag, as shown in Figure 3 (c).

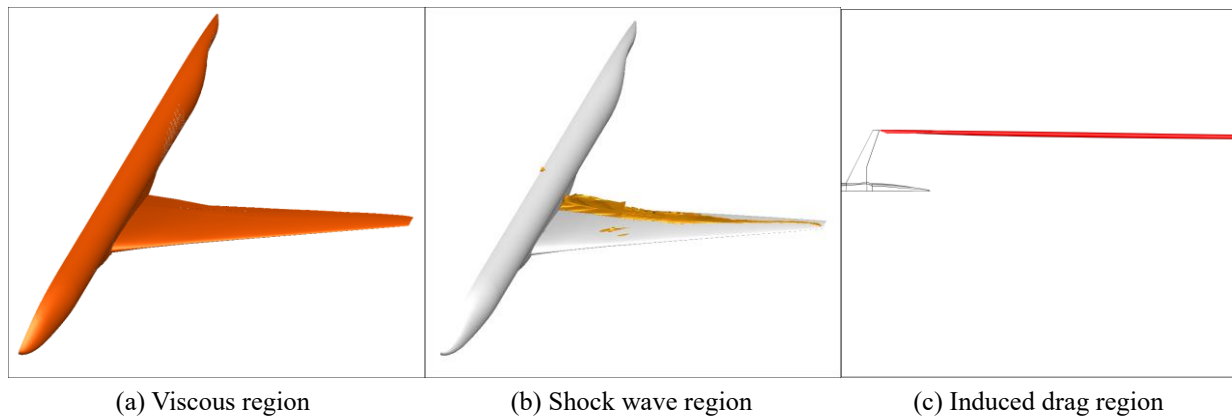


Figure 3: Drag integral region

The two-dimensional airfoil NACA0012 and three-dimensional wing-body model DLR-F6 FX2B are used for verifying the far-field drag decomposition method. The calculation results are shown in Figure 4 (a) and (b) [18] [19]. The results show the drag decomposition method is able to calculate wave drag and total accurately and is robust to the change of grid size.

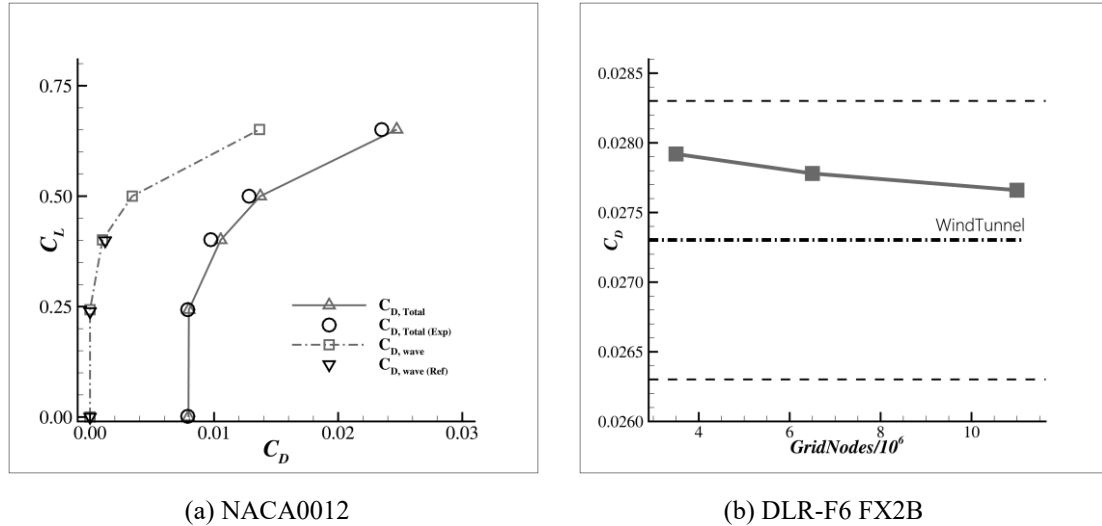


Figure 4: Results of examples verification

3. Numerical Simulation and Discussion

3.1 Research of two-dimensional airfoil

A supercritical airfoil is used for two-dimensional study, as shown in Figure 5. The deflection angle of flaps are restricted with $[-1.0\text{deg}, 1.0\text{deg}]$. The variable-camber airfoil is studied under different lift coefficient and Mach number. The calculating conditions are shown in Table 1. The original airfoil is calculated first under this flight conditions. Then the aerodynamic characteristics of the variable-camber airfoil are analyzed. The original performance of the airfoil and its best variable-camber performance under each flight conditions are shown in Figure 6 (a) and Figure 6 (b). The lift-drag ratio of the airfoil improves in a large range of flight conditions with flap rotation, which proves the benefit of variable-camber technology.

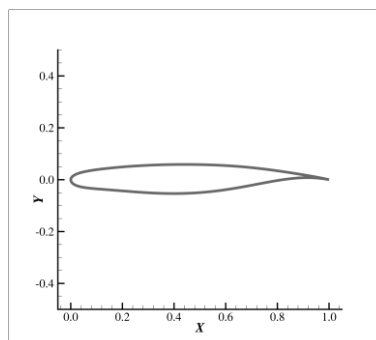


Figure 5: Airfoil geometry

Table 1: Calculating condition

Mach Number	0.70 – 0.76
Lift Coefficient	0.70 – 0.85
Reynolds Number	6.5×10^6

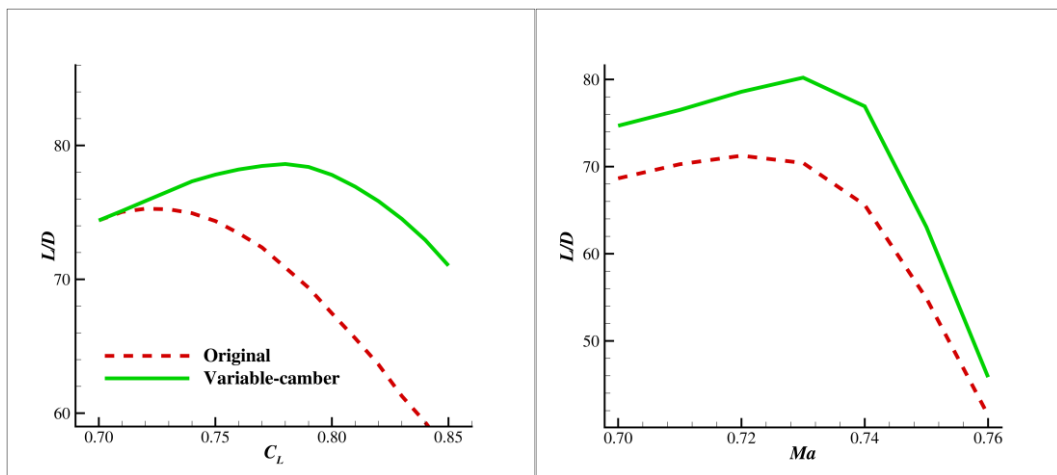
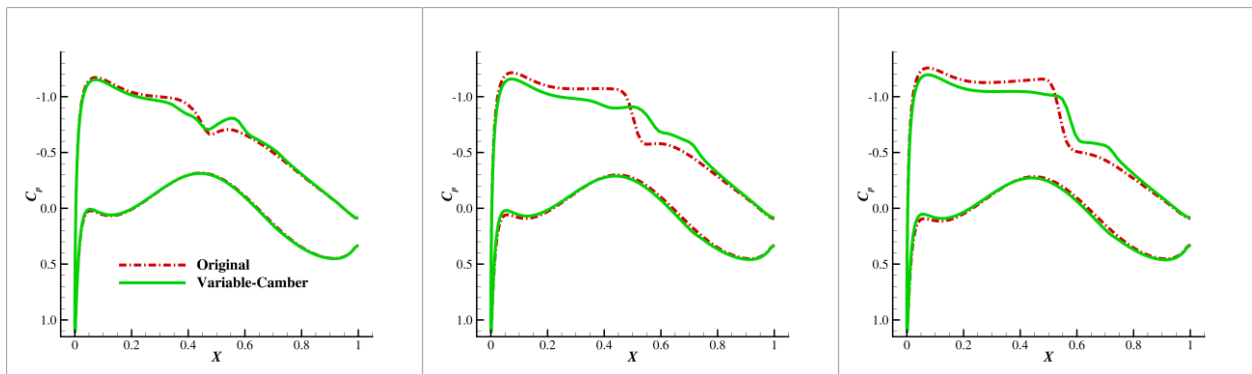
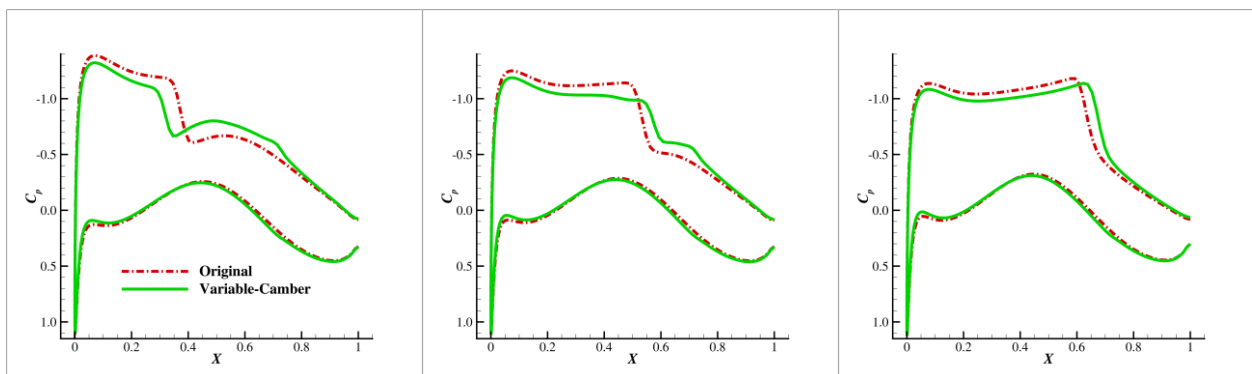
(a) Case1: constant Ma (b) Case2: constant C_L

Figure 6: Comparison between original airfoil and variable-camber airfoil

The pressure distribution under some flight conditions are shown in Figure 7 and Figure 8. The variable-camber airfoil weakened the shock wave, obviously, which means the variable-camber technology can influence wave drag. However, the change of other drag components are still unknown. Consequently, the drag decomposition method will be used in the following part for analyzing.

(a) $C_L=0.72$ (b) $C_L=0.77$ (c) $C_L=0.82$ Figure 7: Pressure distribution of Case1 ($Ma=0.74$)(a) $Ma=0.72$ (b) $Ma=0.74$ (c) $Ma=0.76$ Figure 8: Pressure distribution of Case2 ($C_L=0.81$)

The aerodynamic characteristics of the variable-camber airfoil is analyzed in two cases. Case1 keeps $Ma=0.74$, while case2 keeps $C_L=0.81$. Drag decomposition method is used for studying the drag components. For two-dimensional airfoil, aerodynamic drag is consist of friction drag, form drag and wave drag.

For case1, the airfoil is studied under three different lift coefficient. The drag decomposition results are shown in Figure 9. Figure 9 (a), (b) and (c) shows the change of friction drag, form drag and wave drag, respectively. The friction drag is almost unchanged under three flight conditions. The form drag and wave drag change significantly.

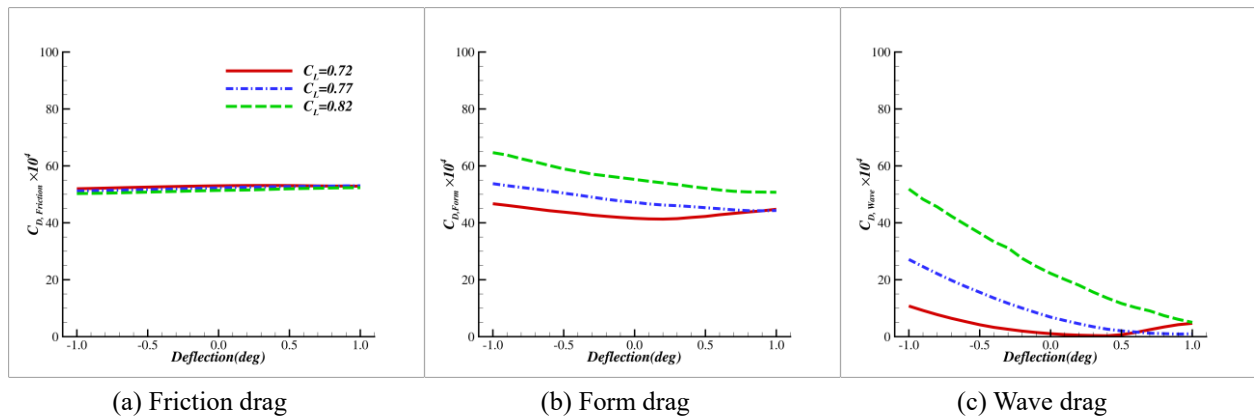


Figure 9: Drag decomposition results of Case1

For the second case, the airfoil is studied under three different Mach number, as shown in Figure 10. The change of friction drag is minor, which is shown in Figure 10 (a). The form drag and wave drag change significantly in Figure 10 (b) and (c), respectively. The change of wave drag is more obvious than form drag. Although the value of different drag components is different under different flight conditions, but the influence of variable-camber technology on drag components is very similar.

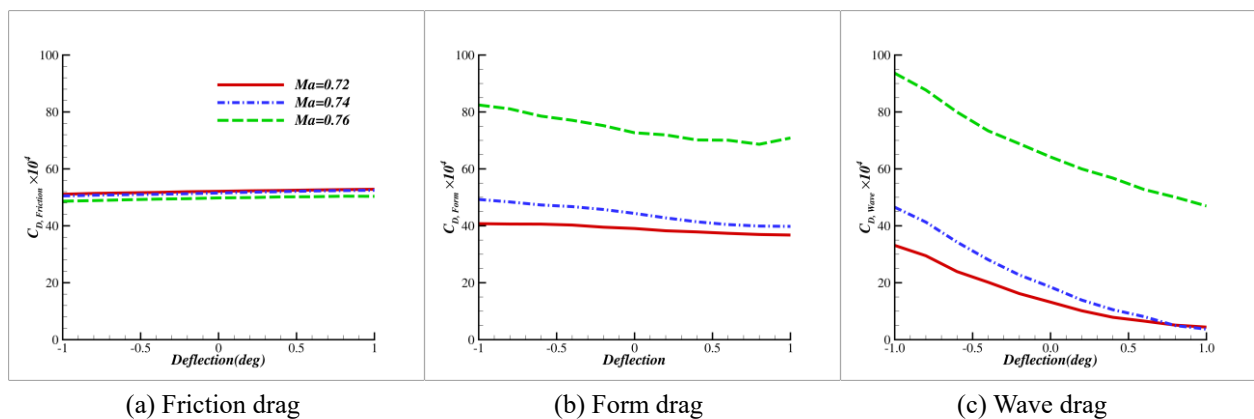


Figure 10: Drag decomposition results of Case2

The result reveals the fact that trailing-edge variable-camber technology improves aerodynamic performance by affecting the wave drag and form drag. The technology is more effective when Mach number or lift coefficient is high, because the wave drag is sensitive to change of lift coefficient and Mach number, and the airfoil usually has much more wave drag reduction under high lift coefficient. The results give us an idea to utilize the technology. Different flight conditions usually have different requirement on the aerodynamic geometry. The designers can pay more attention to the flight conditions like cruise, whose Mach number and lift coefficient is not too large. The variable-camber technology can be used to improve the performance of high Mach number or high lift coefficient condition,

like the buffet condition or drag divergence condition.

3.2 Research of three-dimensional wing

The research on two dimensional airfoil avoids the interference of cross-flow and reveals the two-dimensional effect of trailing-edge variable-camber wing technology. However, the three-dimensional flow is much complex than two-dimensional flow. Consequently, the research on three-dimensional variable-camber wing is essential.

The wing used for study is shown in Figure 2. The geometry of the wing is controlled by seven sections. The section 4, 5, 6 and 7 are the supercritical airfoil we studied in two dimensional research. Due to the huge time consuming of three-dimensional numerical simulation, we only studied the aerodynamic characteristics of variable-camber wing in cruise condition. The calculation condition is shown in Table 2. The aerodynamic drag of the airplanes is composed of friction drag, form drag, wave drag and induced drag. The two-dimensional study shows the change of friction drag and form drag is small comparing to wave drag. Thus we will neglect friction drag and form drag, and focusing on the wave drag and induced drag.

Table 2: Calculating condition

Mach Number	0.85
Reynolds Number	5.3×10^7
Lift Coefficient	0.50

The civil airplanes usually have two individual flaps. This paper studied the influence of different flaps separately. The inner flap is studied first. When rotating the inner flap, the outer flap keeps a constant deflection angle. Then the outer flap deflects while keeping the inner flap fixed. The research calculated the variable-camber wing with 39 different trailing-edge camber, and the results are shown in Figure 11. Figure 11 (a) shows the impact of inner flap rotation. The inner flap rotate within the interval of $[-0.6\text{deg}, 0.6\text{deg}]$. The drag coefficient is less affected by the rotation of inner flap. Figure 11 (b) shows the drag coefficient of variable-camber wing when rotating the outer flap. The drag coefficient change obviously when outer flap deflecting. That is to say, the outer flap is more effective in drag reduction.

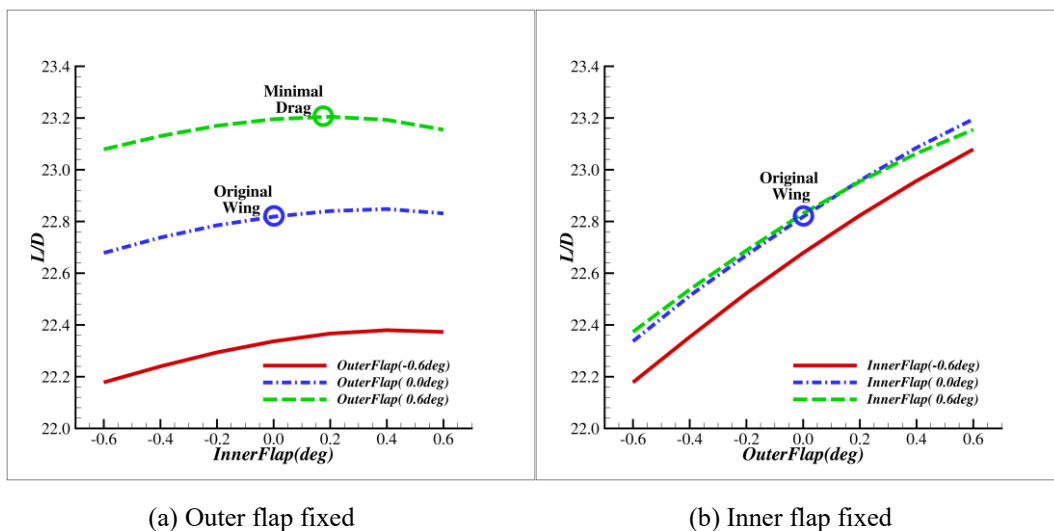


Figure 11: Lift-drag ration of variable-camber wing

The variable-camber wing with 0.2deg inner flap deflection and 0.6deg outer flap deflection has the lowest drag coefficient. A comparison between original wing and minimal drag wing is made, and their pressure distributions are shown in Figure 12. The 23% spanwise section pressure distribution in Figure 12 (a) shows the variable-camber wing

has slightly weakened the shock wave and suction peak, but has little impact on other flow structure. Figure 12 (b) shows the pressure distribution at 46% spanwise section, where the shock wave has almost disappear with trailing edge rotation. The pressure distribution at 69% and 91% spanwise section are shown in Figure 12 (c) and Figure 12 (d). The shock wave of variable-camber wing becomes stronger at these sections. It is hard to estimate whether the wave drag increases or decreases.

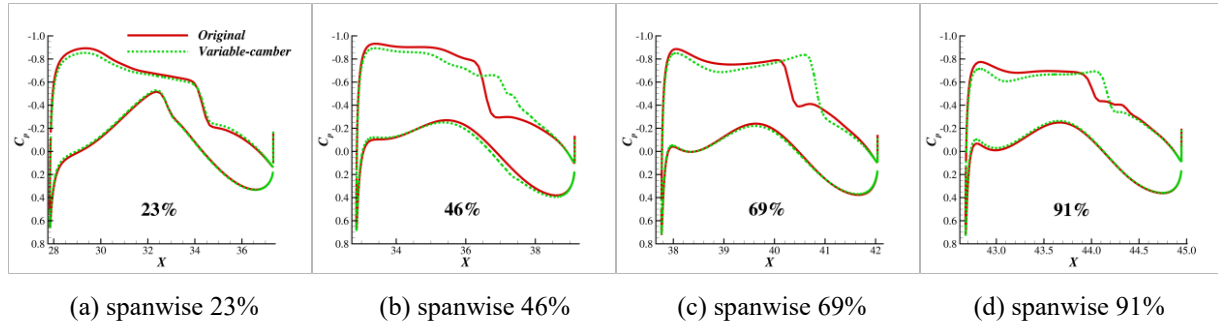


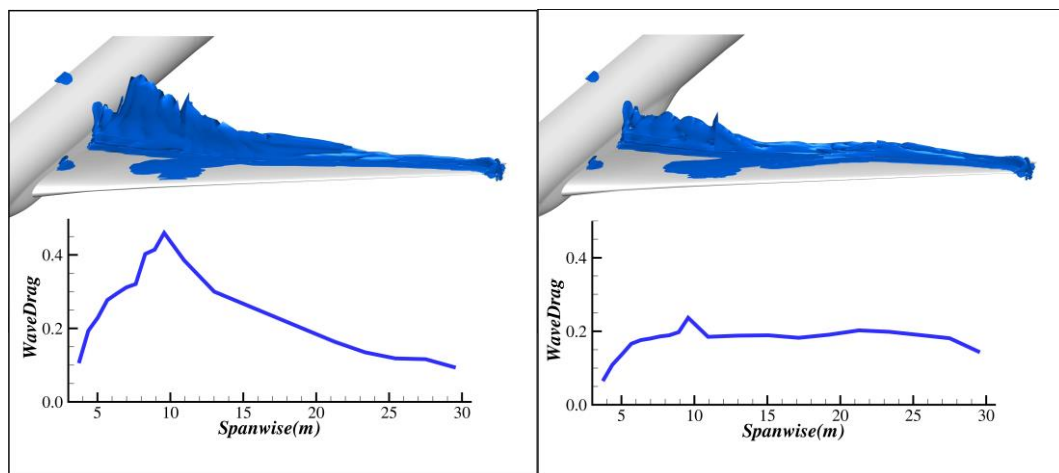
Figure 12: Pressure distribution of variable-camber wing and original wing

The CFD results reveals the trailing-edge variable-camber wing has 0.00035 reduction of drag coefficient, but it is uneasy to analyze the drag reduction mechanism of variable-camber technology. Thus, the drag decomposition method is applied for the three-dimensional wing. The drag decomposition results of original wing and minimal drag wing are shown in Table 3.

Table 3: Drag decomposition results

	Total Drag	Viscous Drag	Induced Drag	Wave Drag
Original	0.02191	0.01227	0.00873	0.00091
Minimal Drag	0.02156	0.01223	0.00866	0.00067

The optimal variable-camber wing has 0.00035 drag reduction (1.5% of total drag) comparing to the original wing. The reduction of wave drag and induced drag are 0.00024 and 0.00007. The change of viscous drag (which includes friction drag and form drag) is minor. The wave drag has the largest proportion in total drag reduction. The drag decomposition method is based on the volume integral. Consequently, it is easy to analyze the change of wave drag at different spanwise section. The analyzing result is shown in Figure 13.



(a) Original wing

(b) Minimal drag wing

Figure 13: Wave drag distribution

The wave drag of inner part and middle part of wing has reduced, while the outer part wave drag increased. The inner part has the largest wave drag reduction, which is conflicted with the pressure distribution change in Figure 12. The comparison leads to a conclusion, that the inner part of wing is more sensitive to the change of wave drag. The small change of shock wave at inner part will lead to great change in wave drag.

The drag decomposition method is applied to all 39 variable-camber wing to analyze the changing rule of wave drag. The results are shown in Figure 14. Figure 14 (a) and (b) is the variance of wave drag with the deflection of inner and outer flaps, respectively. The inner and outer flaps almost has the same influence on wave drag. By deflection the flaps downward, the trailing-edge variable-camber wing can effectively weaken the shock wave and reduce the wave drag.

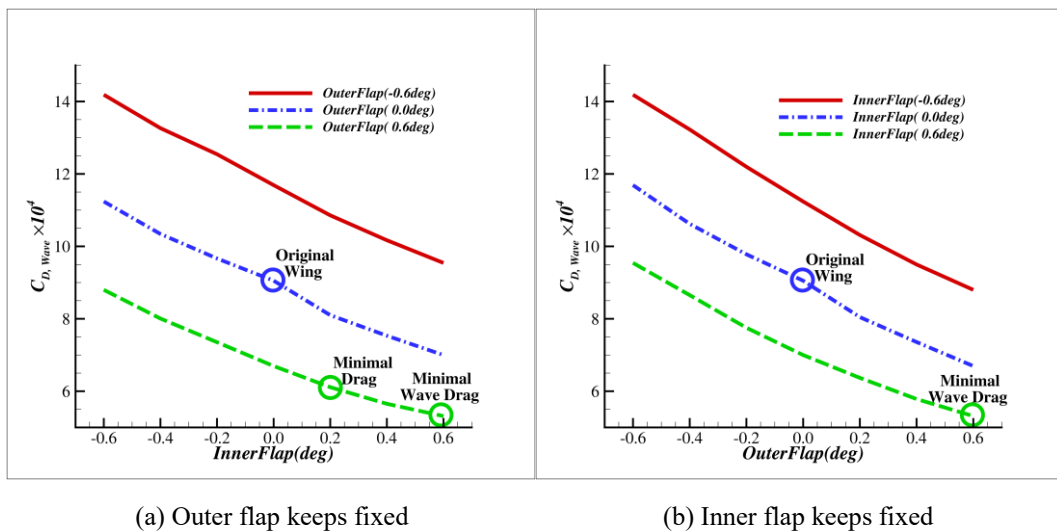


Figure 14: Drag decomposition results of wave drag

Although the minimal drag variable-camber wing reduces little induced drag, but it still shows the variable-camber wing has the ability to influence induced drag. In Figure 15 (a) and (b), the variance of induced drag shows the variable-camber wing can further reduce the induced drag by deflecting the inner flap upward and deflecting the outer flap downward. The inner flap and outer flap have opposite influence on induced drag, and the inner flap has larger influence than outer flap.

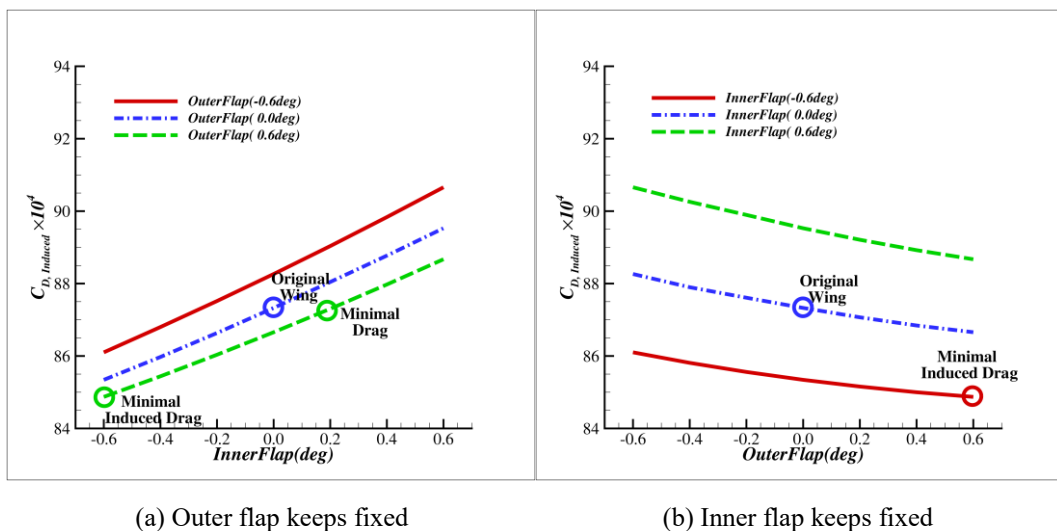


Figure 15: Drag decomposition results of induced drag

From the drag decomposition results, we find the wing of with [0.6deg, 0.6deg] (two rotation angle refer to the inner flap and outer flap, respectively) trailing-edge deflection has the smallest wave drag, and the wing with [-0.6deg, 0.6deg] trailing-edge deflection has the smallest induced drag. The minimal drag wing (whose deflection angle is [0.2deg, 0.6deg]) has different geometry with the two wings above. The results indicate that variable-camber wing with lowest drag coefficient is the result of compromising, the reduction of wave drag and induced drag is contradicted with each other to some extent.

4. Conclusion

This paper studied the aerodynamic characteristics of trailing-edge variable-camber wing technology. A drag decomposition method and CFD is used for numerical simulation. The research of two-dimensional supercritical airfoil reveals the impact of variable-camber airfoil to friction drag, form drag and wave drag. The wave drag is proved to be the main drag reduction for two-dimensional variable-camber technology. The three-dimensional study shows the influence of trailing-edge camber of wing on the total drag, wave drag and induced drag. The conclusion will be helpful for the further study and design of variable-camber wing.

Reference

- [1] OLASON L., and NORTON A. Aerodynamic design philosophy of the Boeing 737. AIAA Paper, 1965, No. 65-739, pp. 1-30.
- [2] Dudley J., Huang X., and Macmillin P. Multidisciplinary Optimization of the High-Speed Civil Transport. 33rd Aerospace Sciences Meeting & Exhibit, 1995, Reno, Nevada.
- [3] Goldhammer, M. The Next Decade in Commercial Aircraft Aerodynamics—A Boeing Perspective. Aerodays 2011, Madrid, Spain, 2011.
- [4] Nhan N., Eric T., Sean S., and Abraham I. Distributed Parameter Optimal Control by Adjoint Aeroelastic Differential Operators for Mode Suppression Control. AIAA Guidance, Navigation, and Control (GNC) Conference, 2013, Boston, MA.
- [5] David J., and Brian J. Lift Distributions for Minimum Induced Drag with Generalized Bending Moment Constraints. JOURNAL OF AIRCRAFT, 2013, Vol. 50, No. 3, pp. 936-946.
- [6] Gustavo E., and Nhan N. Adaptive Aeroelastic Wing Shape Optimization for High-Lift Configurations. 33rd AIAA Applied Aerodynamics Conference, 2015, Dallas, TX.
- [7] Alexander B., and Glenn B. Estimated Benefits of Variable-Geometry Wing Camber Control for Transport Aircraft. Technical Memorandum, NASA Dryden Flight Research Center, Edwards, CA, NASA/TM-1999-206586.
- [8] Marques M., Gamboa P., and Andrade E. Design of a Variable Camber Flap for Minimum Drag and Improved Energy Efficiency. 50th AIAA/ASME/ASCE/AHS/ASC Structures, Structural Dynamics, and Materials Conference, 2009, Palm Springs, California.
- [9] Zhoujie L., and Joaquim R. Aerodynamic Shape Optimization of an Adaptive Morphing Trailing-Edge Wing. JOURNAL OF AIRCRAFT, 2011, Vol. 48, No. 6, pp. 1951-1970.
- [10] Yaolong L., and Eike S. Variable Camber Application to Aircraft in Formation Flight. 54th AIAA Aerospace Sciences Meeting, 2016, San Diego, California, USA.
- [11] Michael W. Application of an Adaptive Shock Control Bump for Drag Reduction on a Variable Camber NLF Wing. 2018 AIAA Aerospace Sciences Meeting, 2018, Kissimmee, Florida.
- [12] Jae-Sung B., Michael S., and Daniel J. Aerodynamic and Static Aeroelastic Characteristics of a Variable-Span Morphing Wing. JOURNAL OF AIRCRAFT, 2005, Vol. 42, No. 2, pp. 528-534.
- [13] Joel A., Russell F., Sridhar K., Peter M., and Donald B. Flight Testing of Mission Adaptive Compliant Wing. 48th AIAA/ASME/ASCE/AHS/ASC Structures, Structural Dynamics, and Materials Conference, 2007, Honolulu, Hawaii.
- [14] Yan L., Jun L., Honggang Z., Bo L., Nan L., and Junqiang B., Robust Optimization of Variable-Camber Continuous Trailing-Edge Flap System under Multi-Task Profiles. 35th AIAA Applied Aerodynamics Conference, 2017, Denver, Colorado.
- [15] Papanone L., Tognaccini R., and Papanone L. Computational Fluid Dynamics-Based Drag Prediction and Decomposition. AIAA JOURNAL, 2003, Vol.41, No.9, pp. 1647-1657.
- [16] Kevin A. Lane and David D. Marshall. Inverse Airfoil Design Utilizing CST Parameterization. 48th AIAA

- Aerospace Sciences Meeting Including the New Horizons Forum and Aerospace Exposition, January 2010, Orlando, Florida.
- [17] Lanzetta M., Mele B., and Tognaccini R. Advances in Aerodynamic Drag Extraction by Far-Field Methods. JOURNAL OF AIRCRAFT, 2015, Vol.52, No.6, pp. 1873-1886.
- [18] McCroskey W J. A critical assessment of wind tunnel results for the NACA 0012 airfoil[R]. NATIONAL AERONAUTICS AND SPACE ADMINISTRATION MOFFETT FIELD CA AMES RESEARCHCENTER, 1987.
- [19] Gregory M., Melissa B., Scott L., Ralf R., and Martin S. Experimental Investigation of the DLR-F6 Transport Configuration in the National Transonic Facility (Invited). 26th AIAA Applied Aerodynamics Conference, August 2008, Honolulu, Hawaii.